Int J Adv Manuf Technol (2013) 68:2133–2144
DOI 10.1007/s00170-013-4831-2

ORIGINAL ARTICLE

An iterative numerical method for determination of temperature-dependent friction coefficients in thermomechanical model analysis of cold bolt forging

U. Ince · M. Güden

Received: 7 November 2012 / Accepted: 3 February 2013 / Published online: 20 February 2013

Abstract A set of temperature-dependent friction coefficients was developed to increase the accuracy of finite element (FE) simulations of cold bolt forging. The initially attained friction coefficients at different temperatures were calibrated with the iterations between the experimental and thermomechanical model extrusion test loads. The constant friction coefficient and the determined set of friction coefficients as function of temperature were then implemented to the simulations of the cold bolt-forging processes. Further calibrations and model validations were made based on the temperature measurements of the workpiece in the actual bolt-forging processes. To show the advantages of developed temperature-dependent friction coefficients, the loads of four different bolt-forging processes were compared with the thermomechanical model loads calculated using the constant friction and temperature-dependent friction coefficients. The modeling results indicated that the use of temperature-dependent friction coefficients in the FE simulations resulted in nearer temperature distributions and the loads of the workpiece during forging as compared with the use of a constant friction coefficient.

Keywords Friction · Cold forging · Bolt · Numerical simulation · Fastener

U. Ince
Norm Fasteners Co, Atatürk Organize Sanayi Bölgesi 10007,
35620 Çiğli, İzmir, Turkey

M. Güden
Dynamic Testing and Modeling Laboratory,
Izmir Institute of Technology, Gulbahce Koyu,
Urla, Izmir, Turkey

M. Güden (✉)
Department of Mechanical Engineering,
Izmir Institute of Technology, Gulbahce Koyu,
Urla, Izmir 35430, Turkey
e-mail: mustafaguden@iyte.edu.tr

1 Introduction

The friction between workpiece and tool in cold forging directly affects tool stress, material flow, internal defect formation, forging loads, and energy requirements. Previous studies of friction models were mostly based on ring compression and forward and backward rod extrusion tests in conjunction with the inverse analyses of the experimental and numerical simulation results. Hayhurst and Chan [1] proposed a two-parameter friction model (the Coulomb friction model and friction factor yield stress model), which was calibrated by cylindrical and ring compression tests. Behrens and Schafstall [2], using the neural network technique, determined the dependency of friction on contact parameters. The insertion of local friction parameters in the finite element model calculations resulted in higher degree of simulation accuracies. Cho and Altan [3] introduced an inverse analysis technique to determine the friction at tool–workpiece interface at elevated temperatures using the geometrical changes of deformed samples. The technique was capable of determining the flow stress and friction factor simultaneously from one set of tests. Wang et al. [4] reported a real-time measurement technique of evaluating the friction in a ring test. Cora et al. [5] investigated the effect of constant and variable friction coefficients in cold forging. The constant friction coefficient was shown to not able to capture the actual friction conditions. Tan et al. [6] investigated the friction stresses under different pressures and reported a linear relationship between normal pressure and friction stress. Dubois et al. [7] conducted upsetting–sliding test between 25 and 150 °C on a zinc phosphate/soap-coated carbon steel to simulate the characteristic contact conditions in a cold heading sequence composing of wire drawing and direct extrusion. The friction coefficient decreased from 0.071 to 0.04 when the temperature

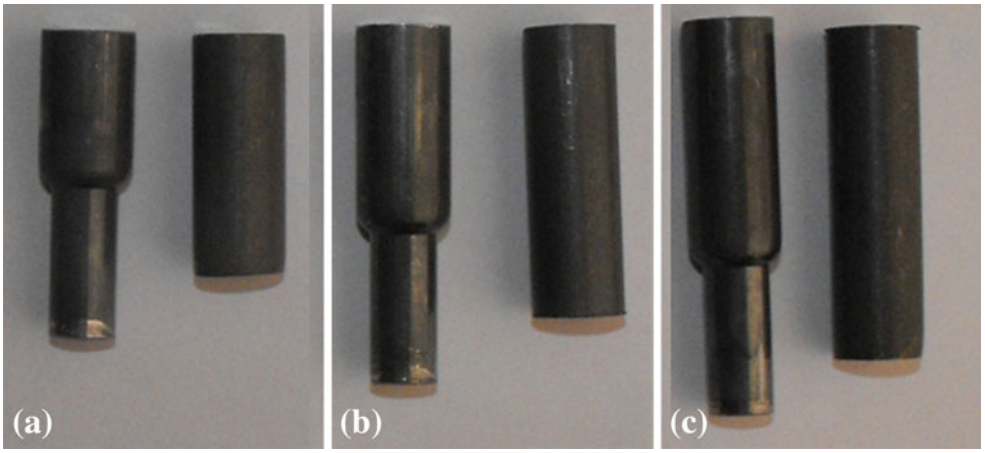

Fig. 1 QST36-3 steel samples after and before forward extrusion test; specimens **a** 25 mm, **b** 30 mm, and **c** 35 mm in length

increased from 25 to 150 °C. The drop in the friction coefficient at intermediate temperatures was attributed to the softening and/or melting of sodium and zinc stearates. Saiki et al. [8] investigated the plastic deformation of zinc phosphate-coated specimens and showed that the friction between die and specimen varied with the die geometry and temperature.

In the present study, an iterative numerical method was proposed for the determination of the temperature-dependent friction coefficients in the thermomechanical model analysis of cold bolt forging in order to increases the accuracy of the simulations. The method was based on the determination of friction coefficients as function temperature by means of forward rod extrusion tests and thermomechanical simulations. The surface temperatures of workpieces in actual cold bolt-forging processes were measured using a thermal camera to validate the thermomechanical model. Finally, the forging loads of four different bolt-forging processing, M8×28 plastic screw, M8×16 DIN 6921, M8×30 DIN 6921, and M8×65 convex head, were measured and compared with those of numerical forging loads of the constant and variable friction coefficients.

2 Materials and testing

Forward rod extrusion experiments with the reduction ratios of 48 % were performed using zinc phosphate/soap-coated cylindrical QST36-3 steel samples; 25, 30 and 35 mm in length and 9.73 mm in diameter, as depicted in Fig. 1a–c. The zinc phosphate coating prevents the metal to metal contact and the metal soap reduces the friction between tool and workpiece [9, 10]. Before the extrusion experiments, the die, punch and workpiece were either heated to 120 or 180 °C in a furnace. The surface temperatures of the die, punch, and workpiece were measured in the furnace using a thermal camera before they were taken from the furnace for the extrusion tests. The time elapsed between the start of extrusion test and the moment at which the die, punch, and workpiece taken from the furnace was about 40 s. The extrusion tests were performed in a Schimadzu mechanical testing machine at the displacement rate of 0.05 mms^{-1}. The final displacement attained in the extrusion tests was 12 mm. The displacement was calculated by subtracting the test machine displacement from the total displacement. The machine compliance used to calculate machine displacement was determined in a separate experiment by compressing the compression test platens until about a final prescribed load. Finally, each group of extrusion tests was repeated at least three times and the load values were determined as the average of three experiments.

The emissivity of zinc phosphate-coated QST36-3 steel, which was required in the thermal camera measurements, was determined by applying the following procedure. A black tape with a known emissivity, 0.96, was stuck on the workpiece. The temperature of the black tape with the emissivity number of 0.9 varied between 28.84 and 29.35 °C and the temperature of the workpiece between 28.01 and 28.7 °C. The emissivity of the workpiece was then reduced until the temperature of the workpiece became nearly equal to that of the black tape. Using the aforementioned procedure, the emissivity of the workpiece was found to be 0.79.

Fig. 2 Axisymmetric extrusion die model

3 Modeling, material model parameters, and model validation

The extrusion tests simulations (implicit) were implemented in Simufact®. Three-dimensional solid models of the extrusion die and punch were created in Catia V5 software. The axisymmetric extrusion die model is shown in Fig. 2 and composed of stress ring, insert, space holder, case, steel blocks, and locking nut. The extrusion die and workpiece were modeled using Quad-4 solid elements. The size and number of the elements used in the extrusion die models were sequentially 0.2 mm and 6,393 for the inserts, 0.4 mm and 2,407 for the punch, 0.4 mm and 2,894 for the front stress ring, 0.4 mm and 3,188 for the back stress ring, 0.8 mm and 2,281 for the case, 0.4 mm and 4,165 for the steel blocks, and 0.8 mm and 1,204 for the nut. The workpiece was modeled with 0.2 mm element size and the numbers of elements used in 25, 30, and 35 mm long workpieces were sequentially 3,140, 3,777, and 4,406.

The die components were modeled with an elastic material model. The simulations were performed in accord with the extrusion tests: the heated extrusion die, punch, and workpiece were waited in open atmosphere for 40 s before the start of the simulations of the extrusion tests. The die components except inserts were made of 1.2344 tool steel. The Poisson's ratio and mass density of 1.2344 tool steel were 0.23 and 7.85 gcm^{-3}, respectively. The elastic modulus, thermal conductivity, and heat capacity of 1.2344 tool steel were provided by the manufacturer data sheet (Uddeholms AB). The thermal expansion coefficient of 1.2344 tool steel was taken as $1.17\times10^{-5}\,°C^{-1}$ and increased with increasing temperature with a coefficient of $3.01\times10^{-9}\,°C^{-1}$. The thermal conductivity, thermal expansion coefficient and heat capacity of the insert material, WC/Co (19 % Co) PM tool steel, were taken from the manufacturer data sheet (Ceratizit S.A Company). The elastic modulus, Poisson's ratio and mass density of WC/Co PM tool steel were 496 GPa, 0.24 gcm^{-3}, and 12.950 gcm^{-3}, respectively. A Coulomb friction was applied between the workpiece and die in the models and the mechanical and friction heat generation conversion factor was taken as 0.9. The Coulomb friction is given as

$$\sigma_t = -\mu\,\sigma_n \frac{v_s}{|v_s|} \tag{1}$$

where, σ_t is the friction stress, μ is the friction coefficient, σ_n is the contact pressure, and v_s is the sliding velocity.

The workpieces were modeled using the piecewise linear plasticity model. The tensile true stress-strain curve of QST36-3 steel used in the extrusion experiments and 20MnB4 steel used in the actual bolt-forging were determined between 20 and 400 °C at the strain rates of 1, 10, and 50 s^{-1}. The curves were directly entered into the Simufact. Figures 3a and b show true stress-true plastic strain curves of QST36-3 and 20MnB4 steel at various temperatures and strain rates, respectively. The Poisson's ratio and mass density of QST36-3 and 20MnB4 steel were taken as 0.29 and 7.85 gcm^{-3}, respectively. The elastic modulus of QST36-3 and 20MnB4 steel was taken as function of temperature, 212 GPa at 20 °C with a temperature reduction coefficient of 0.096 $GPa°C^{-1}$. The thermal expansion coefficient of QST36-3 and 20MnB4 steel was $1.19\times10^{-5}\,°C^{-1}$ and increased with increasing temperature with a coefficient of $5.6\times10^{-9}\,°C^{-1}$.

The experimental extrusion load–displacement curves were compared to the simulation load–displacement curves of constant and temperature-dependent friction coefficients. The temperature-dependent friction coefficients, which

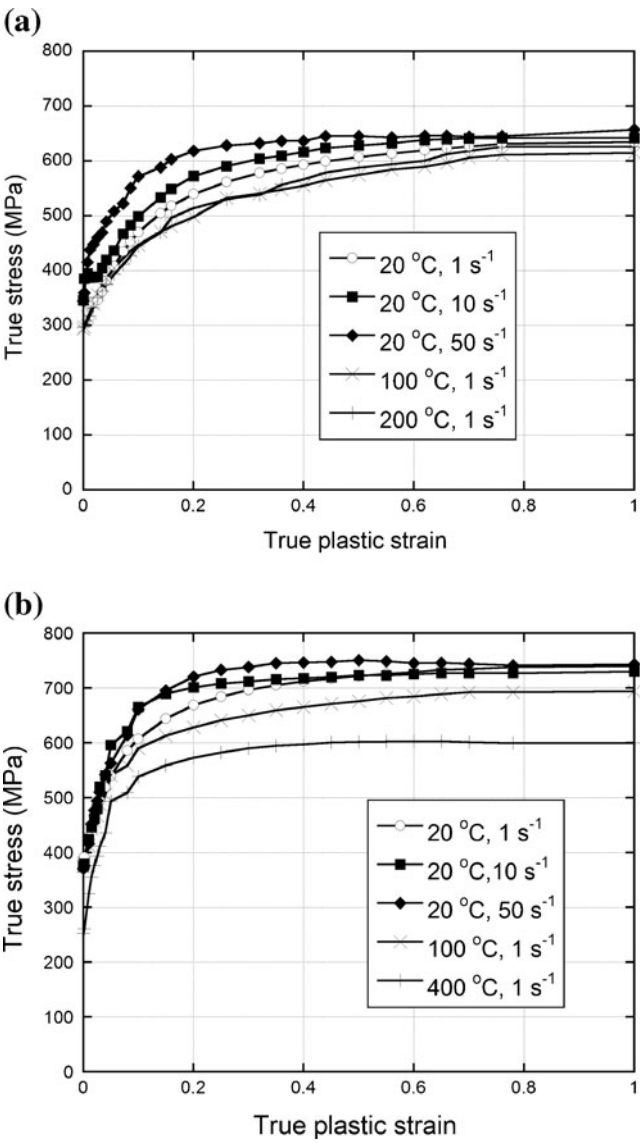

Fig. 3 True stress-true plastic strain curves of **a** QST36-3 and **b** 20MnB4 steel at various strain rates and temperatures

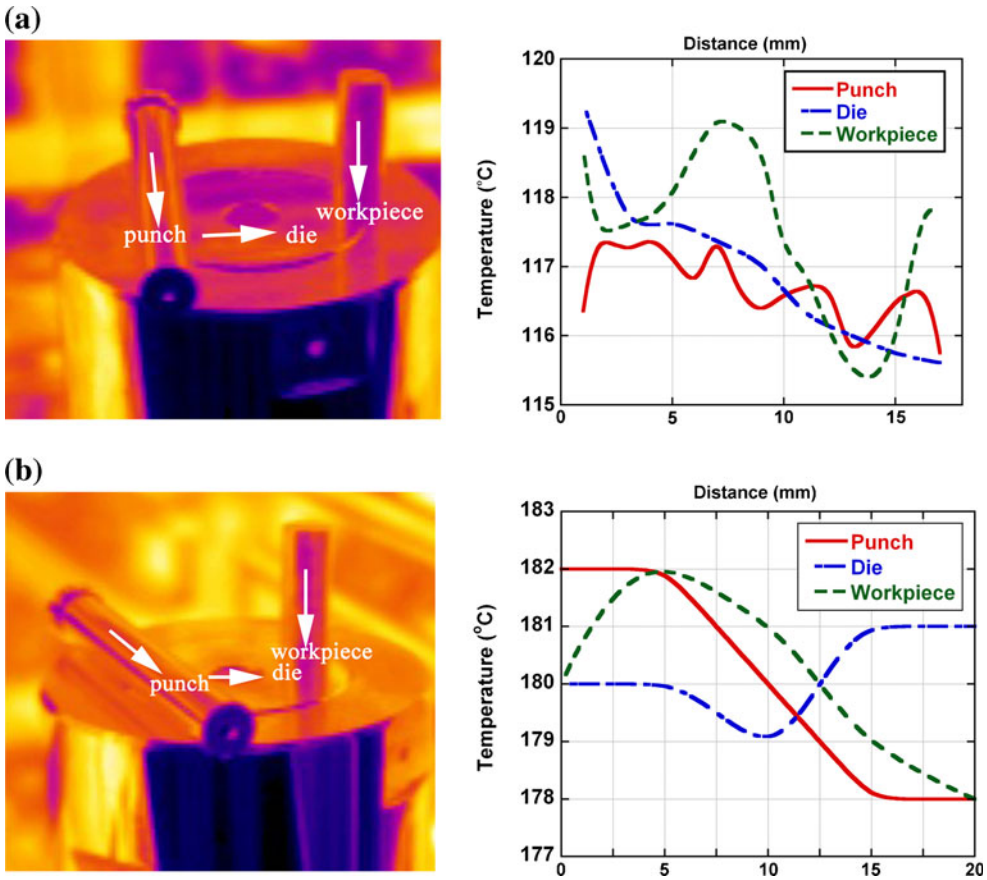

Fig. 4 Thermal camera pictures and the variation of the temperature of extrusion die, punch and workpiece (in the furnace) heated to **a** 120 and **b** 180 °C (the line of measurements are shown by *arrows*)

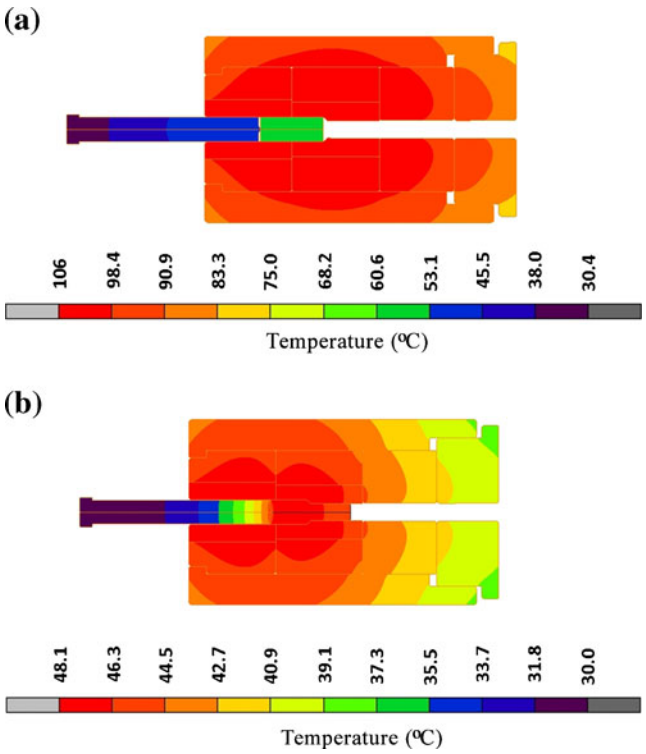

Fig. 5 The temperature distribution of the extrusion die, punch, and workpiece heated to 120 °C; **a** after 40 s taken from the furnace and **b** after the extrusion test (25-mm sample)

nearly approximate the experimental load–displacement curves in the simulations, were identified. The numerically determined temperature-dependent friction coefficients were then implemented to the actual bolt-forging process. M8×20 circular head and M10×20 Inbus DIN 912 cold bolt-forging

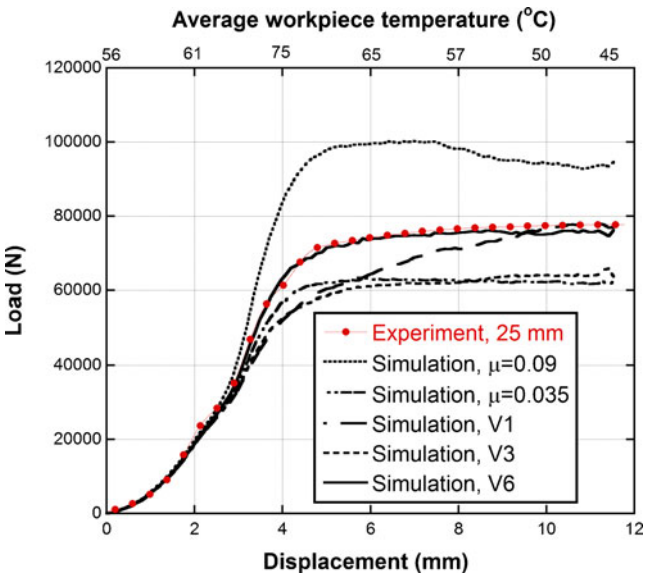

Fig. 6 Experimental and numerical extrusion load–displacement curves with constant and temperature-dependent friction coefficients, 25 mm long sample heated to 120 °C

Table 1 The friction coefficient variation with temperature in various scenarios

T(°C)	V1	V2	V3	V4	V5	V6	V7	V8
25	0.090	0.090	0.090	0.090	0.090	0.090	0.090	0.090
50	0.070	0.040	0.040	0.034	0.040	0.065	0.065	0.065
60	–	–	0.035	0.031	–	0.060	0.060	0.060
70	0.035	0.035	0.030	0.028	0.050	0.056	0.055	0.055
75	0.025	0.025	0.025	0.025	0.045	0.050	0.050	0.050
90						0.045	0.045	0.045
105							0.040	0.040
200							0.035	0.035
300								0.0475
400								0.060

processes were performed in a commercial SP300 horizontal crank press in order to compare the measured and numerically determined temperature distributions. M8×28 plastic screw, M8×16 DIN 6921, M8×30 DIN 6921, and M8×65 convex head bolt-forging were performed in a commercial JBF 13B6S horizontal crank press. The maximum forging loads at each station of JBF 13B6S horizontal crank press were measured using piezoelectric sensors. The sensors were calibrated and fixed on the dies in each station. The same numerical model and material model parameters of extrusion test simulations were also implemented in the modeling of the bolt-forging processes.

4 Results and discussion

Figure 4a and b show thermal camera pictures and the variation of the temperature of the punch, die and workpiece heated to 120 and 180 °C, respectively. The temperature was measured on the punch, die, and workpiece separately, along the lines shown by the arrows in Fig. 4a and b. The camera pictures were taken just before the die, punch, and workpiece taken from the furnace for the extrusion tests. The temperature of the punch, die, and workpiece varies between 115.5–119.5 and 178–182 °C at the furnace-heating temperature of 120 and 180 °C as shown in Fig. 4a and b, respectively. The simulation temperature distribution of the extrusion die, punch and workpiece (25 mm) heated to 120 °C is shown in Fig. 5a before the extrusion test but after 40 s taken from the furnace. As seen in Fig. 5a, the temperature of the workpiece decreases to 60 °C and the temperature of the punch to 30–50 °C after

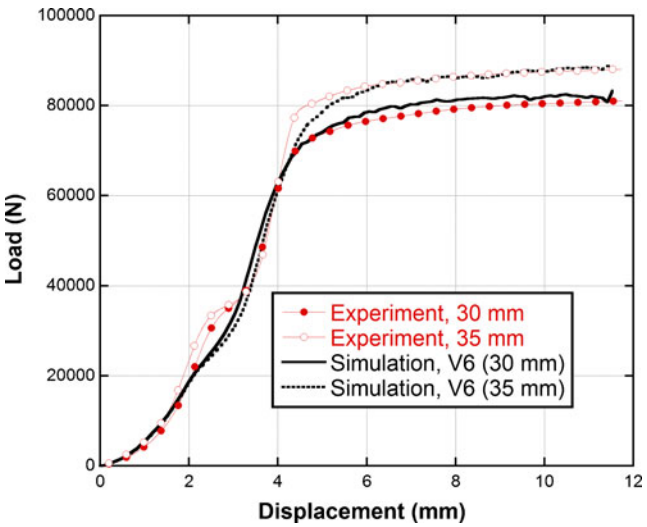

Fig. 7 Experimental and numerical extrusion load–displacement curves of 30 and 35 mm long samples long sample heated to 120 °C

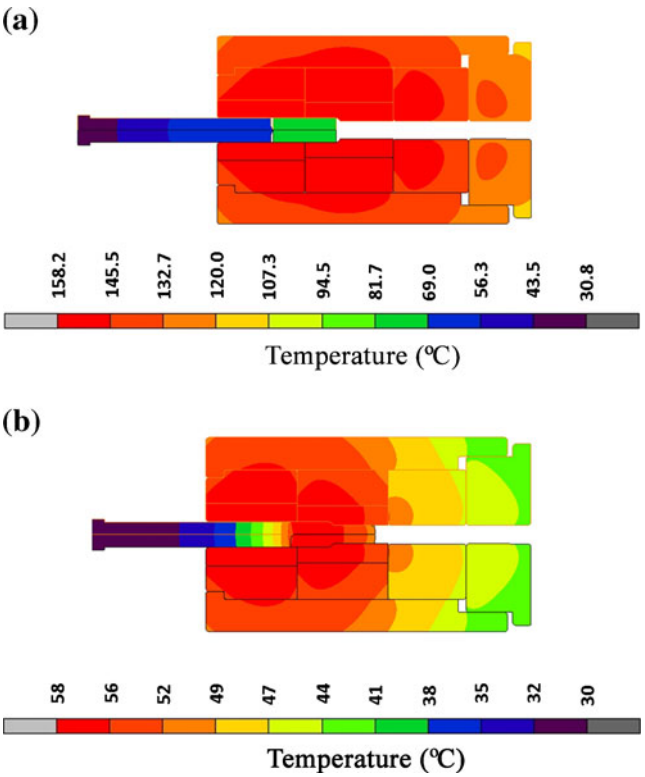

Fig. 8 The temperature distribution of the extrusion die, punch and workpiece heated to 180 °C **a** after 40 s taken from the furnace and **b** after extrusion (25-mm sample)

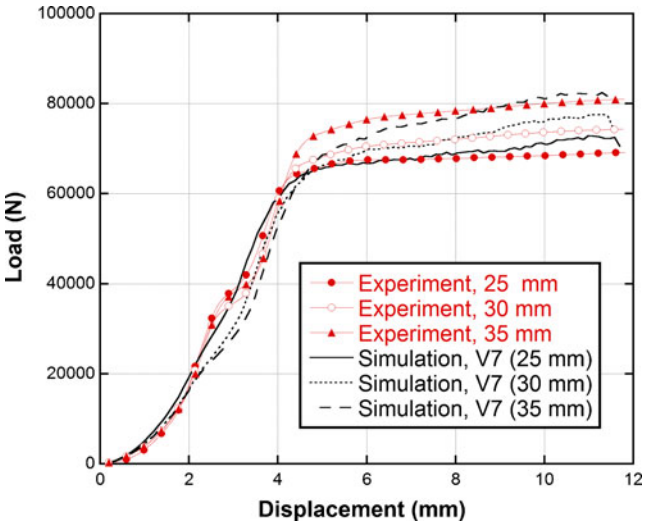

Fig. 9 Experimental and simulation extrusion load–displacement curves of 20, 30 and 35 mm long samples heated to 180 °C

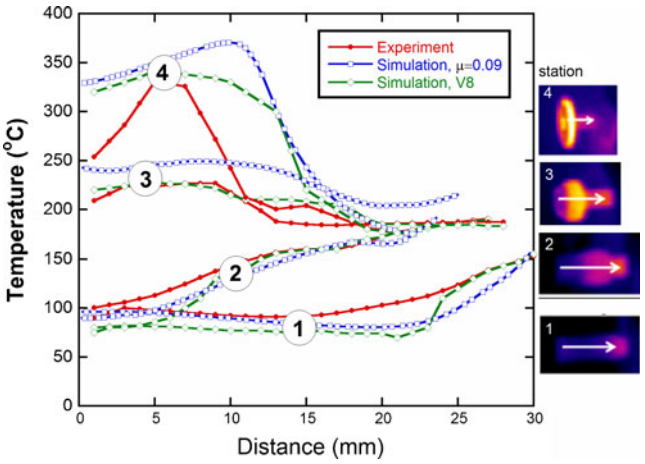

Fig. 11 The experimental (thermal camera) and numerical (constant and V8 set of friction coefficients) temperatures at 4 stations of M8×20 circular head bolt forging (the start and end of the *arrows* show the beginning and end of temperature measurement and the numbers show the station number)

40 s. The simulation temperature distribution of the extrusion die, punch and workpiece after the extrusion test is shown in Fig. 5b for comparison. After the extrusion, the temperature of the workpiece decreases to 40 °C.

The experimental load–displacement curve of 25 mm long specimen heated to 120 °C is shown in Fig. 6 together with numerically determined load–displacement curves using constant friction coefficient (0.09 and 0.035) and temperature-dependent friction coefficients. The constant friction coefficient of 0.09 yields higher, while 0.035 lower extrusion loads than those of experiment. Several different temperature-dependent friction coefficient sets coded as V1, V2, V3, V4, V5, and V6 in Table 1 are developed and implemented. Initially, V1 set of friction coefficients was arbitrarily attained and implemented to the model and then sequentially the friction coefficient set was modified by trial and error until the numerical load–displacement curve

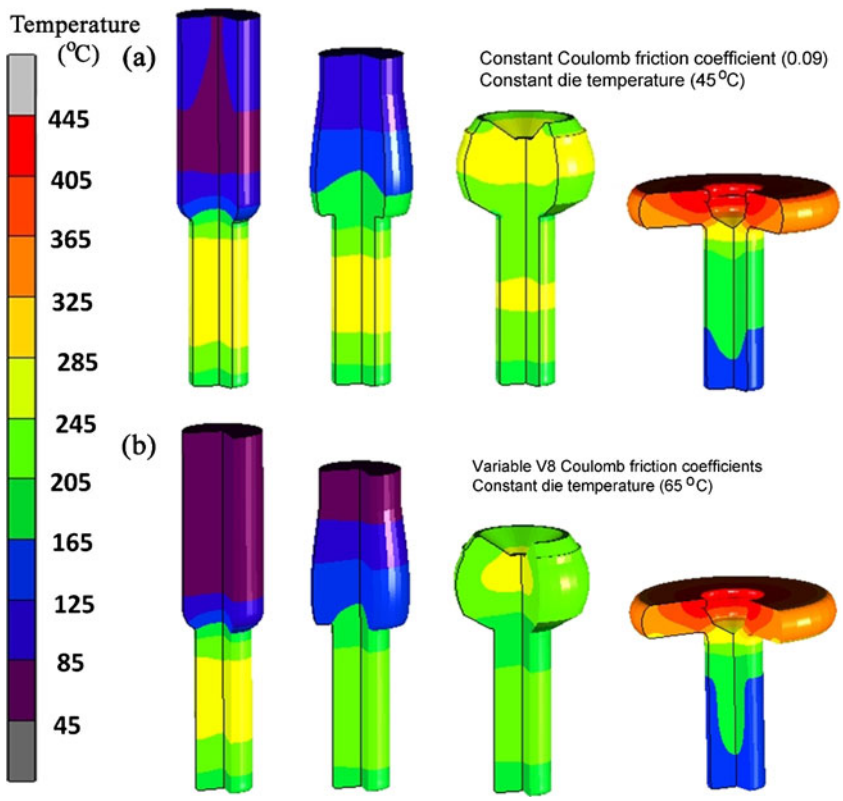

Fig. 10 The simulation temperature distribution of M8×20 circular head bolt forging with **a** constant and **b** temperature-dependent friction coefficients

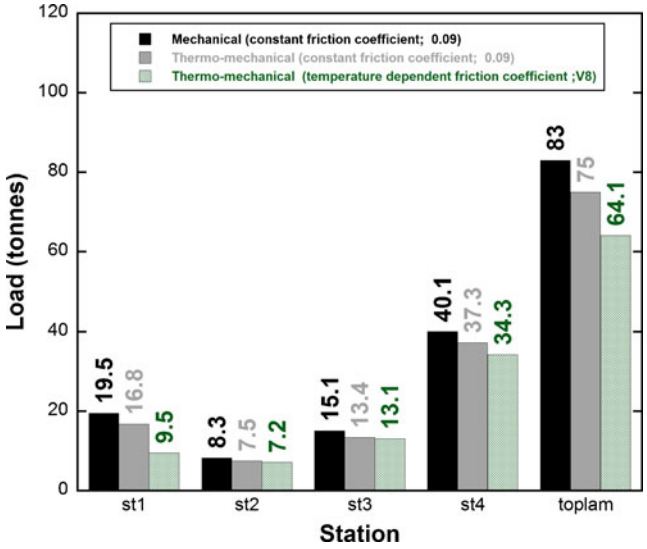

Fig. 12 The numerical press loads of M8×20 circular head bolt forging for constant and temperature-dependent friction coefficients, mechanical, and thermomechanical analysis

attained an acceptable correlation with the experimental load displacement curve (the difference less than 10 %). The load values of V6 set of friction coefficients show the least deviation from the experimental load values as shown in Fig. 6. The extrusion simulations of 30 and 35 mm long samples were implemented using V6 set of friction coefficients. The experimental and simulation load–displacement curves of 30 and 35 mm long workpieces also show very close agreements with each other (Fig. 7). The temperature distributions of the extrusion die, punch and workpiece heated to 180 °C, before and after the extrusion test, are shown in Fig. 8a and b, respectively. The temperature of the workpiece decreases to 50 °C after the extrusion test.

In order to simulate the extrusion of the samples heated to 180 °C, the friction coefficients of set V6 is extended to include the friction coefficient at 200 °C and new set is coded as V7 (Table 1). The simulation extrusion load–displacement curves of 25, 30, and 35 mm long samples using V7 set of friction coefficients are shown in Fig. 9 together with those of experiments. Acceptable agreements are seen between experimental and simulated load–displacement curves of the extruded workpiece heated to 180 °C. The maximum difference between numerical and experimental loads is ~7 %.

The simulations of four-station M8×20 circular head and M10×20 Inbus DIN 912 bolt-forging processes were performed using a constant die temperature in order to simulate the actual forging process, in which after the certain numbers of productions the die temperature reached steady state (constant tool temperature). Figure 10a shows the temperature distribution of M8×20 circular head bolt forging, using the constant friction coefficient of 0.09 and the constant die temperature of 45 °C. As seen in Fig. 10a, the temperature of the workpiece rises above 400 °C in the last station. As zinc phosphate coating layer is expected to break down above 200 °C [11], an increase in the friction coefficient is

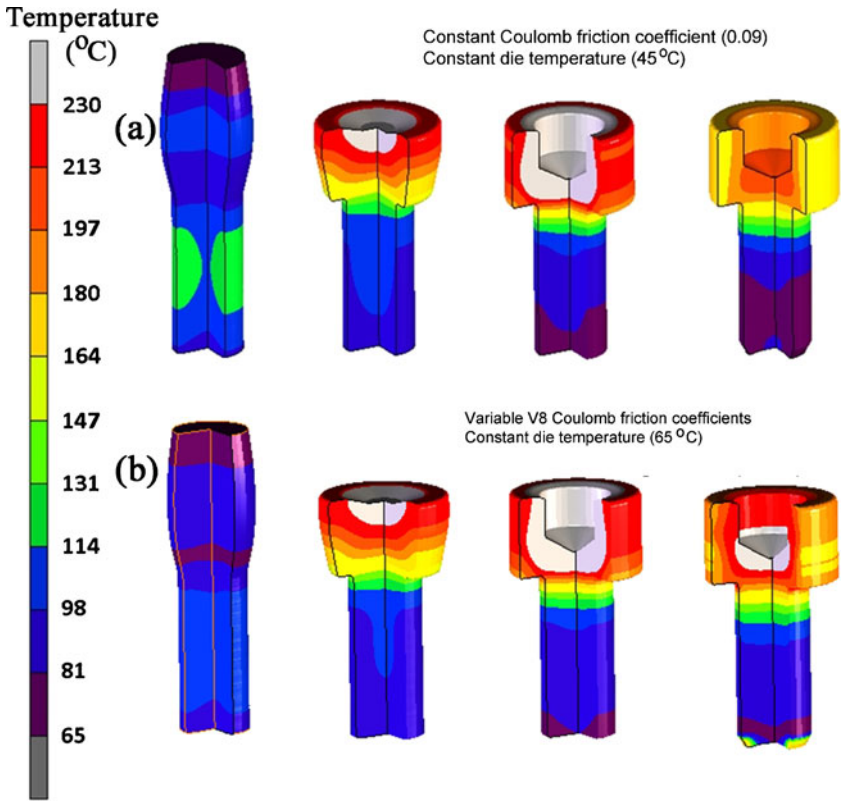

Fig. 13 The temperature distribution of M10×20 DIN 912 Inbus bolt forging with **a** constant and **b** temperature-dependent friction coefficients

naturally expected at elevated temperatures. The simulation and experimental temperature variations of the workpiece at each station are graphically shown in Fig. 11. Constant friction coefficient simulations result in higher temperatures than the measured temperatures (camera) particularly at the third and fourth stations where the workpiece deformations are severe and the deformation temperatures are relatively high. To approximate the measured temperatures at the stations, friction coefficients of 0.0475 and 0.06 at 300 and 400 °C, after several trials and errors, are attained to V7 and new set of friction coefficients is coded as V8 (Table 1). The analysis of the temperature distribution of the workpiece at the stations using V8 set of friction coefficients and the die temperature of 65 °C are shown in Fig. 10b. The temperature distribution of V8 set of friction coefficients show higher degree of correlations with the measured temperature distribution, particularly in the fourth station than that of the constant friction coefficient as shown in Fig. 11. Figure 12 shows the calculated loads in each station using constant friction mechanical and constant and temperature-dependent friction coefficient thermomechanical analysis for comparison. Temperature-dependent friction coefficient thermomechanical analysis results in relatively lower total forging loads than the constant friction mechanical and thermomechanical analysis. The difference between mechanical and thermomechanical analysis, as is expected, increases with increasing workpiece temperature. The decrease in total forging load as compared with mechanical analysis is about 22 % when the temperature-dependent friction coefficients are used in the thermomechanical analysis, while 10 % decrease in load merely results from the use of thermomechanical analysis.

Figure 13a shows the temperature distribution of a 4-station M10×20 Inbus bolt forging using constant friction coefficient of 0.09 and the constant die temperature of 45 °C and Fig. 13b shows the temperature distribution using V8 set of friction coefficients and the constant die temperature of 65 °C. The maximum temperatures in both simulations are about 250 °C. Figure 14a shows the temperature distributions of the first and fourth stations using the constant friction coefficient of 0.09 and the constant die temperature of 45 °C and Fig. 14b shows the temperature distribution of second and third stations using V8 set of friction coefficients and the constant die temperature of 65 °C. The temperature distributions of the stations using V8 set of friction coefficients and the die temperature of 65 °C show again higher degree of correlations with those of experiments than using the constant friction coefficient of 0.09 and the constant die

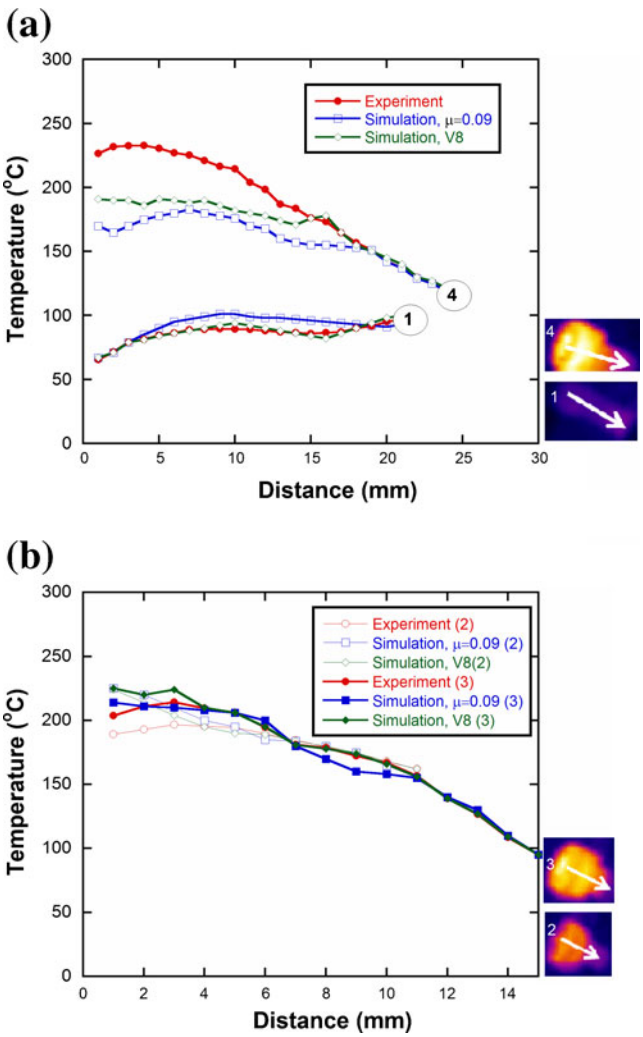

Fig. 14 The experimental (thermal camera) and numerical (constant and V8 set of friction coefficients) temperatures through stations of M10×20 DIN 912 Inbus bolt forging (**a**) stations 1 and 4 and (**b**) 2 and 3 (the start and end of the *arrow* show the beginning and end of temperature measurement and the numbers show the station number)

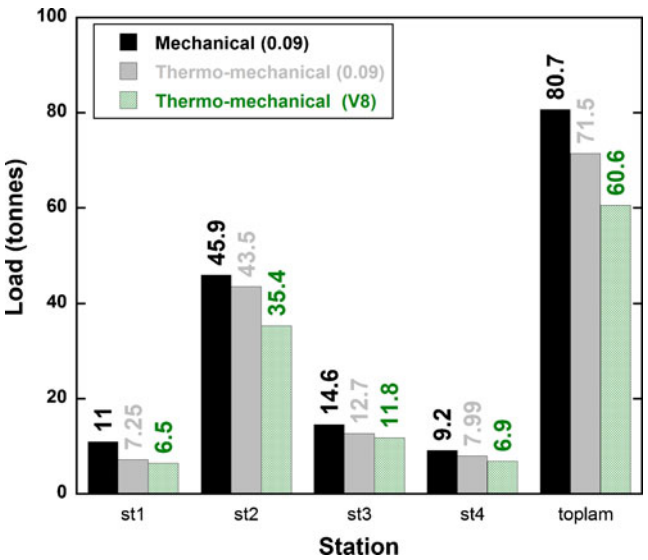

Fig. 15 The numerical press loads of M10×20 DIN 912 Inbus forging for constant and temperature-dependent friction coefficients with mechanical and thermo mechanical analysis

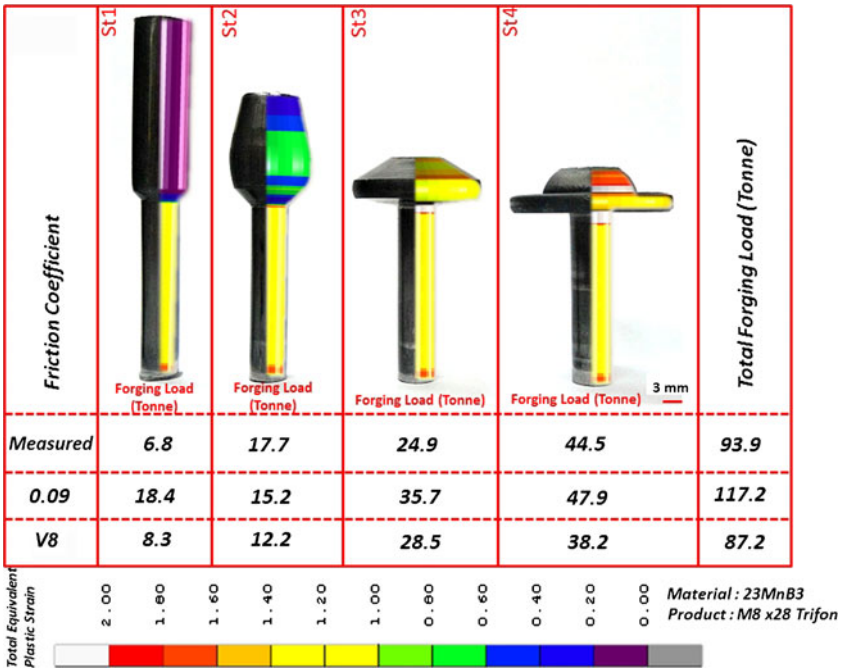

Fig. 16 The equivalent plastic strain distribution, forging loads, and total forging load of M8×28 plastic screw forging process

temperature of 45 °C. As in the M8×20 circular head bolt forging, the variable friction coefficient in M10×20 Inbus bolt forging results in lower total forging load than the constant friction mechanical and thermomechanical analysis as shown in Fig. 15. The decrease in total forging load of temperature-dependent friction coefficient thermomechanical analysis as compared with mechanical analysis is as much as 25 %; 11 % of the decrease results from the use of thermomechanical analysis. These results indicate that the implementation of temperature-dependent friction coefficient in thermomechanical analysis yields lower forging loads than that of constant friction, particularly at the stations of severe plastic deformation.

In order to validate the fidelity of the developed thermomechanical model, the constant friction coefficient and the determined set of friction coefficients were implemented in the thermomechanical analyses of M8×28 plastic screw, M8×16 DIN 6921, M8×30 DIN 6921, M8×65 convex head bolt-forging processes. In the simulations, the maximum forging loads were determined using 0.09 constant friction coefficient, V8 set of temperature-dependent friction coefficients and 65 °C constant die temperature. The results of numerical total plastic strain distribution and measured and numerically determined station forging loads and total forging loads are sequentially shown in Figs. 16, 17, 18, and 19 for M8×28 plastic screw, M8×16 DIN 6921, M8×30 DIN 6921 and M8×65 bolt-

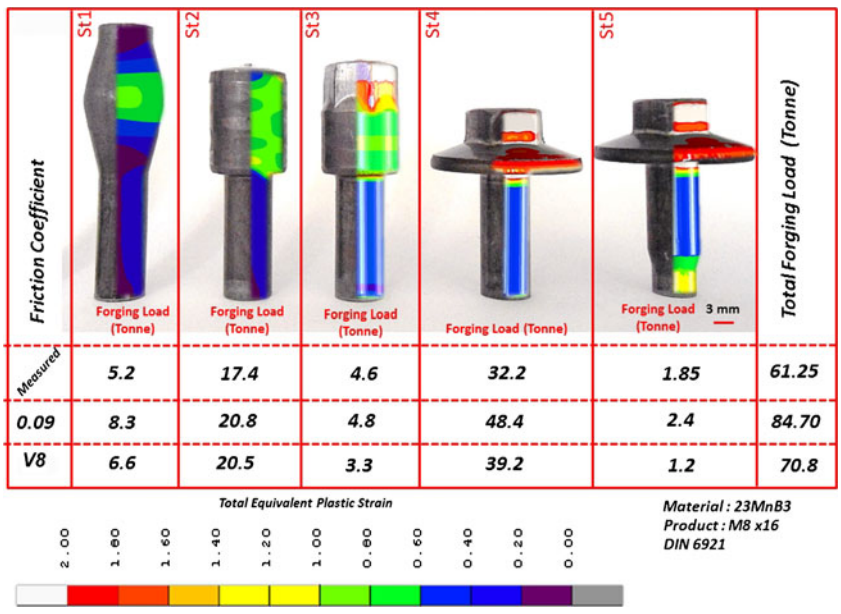

Fig. 17 The equivalent plastic strain distribution, forging loads, and total forging load of M8×16 DIN 6921 forging process

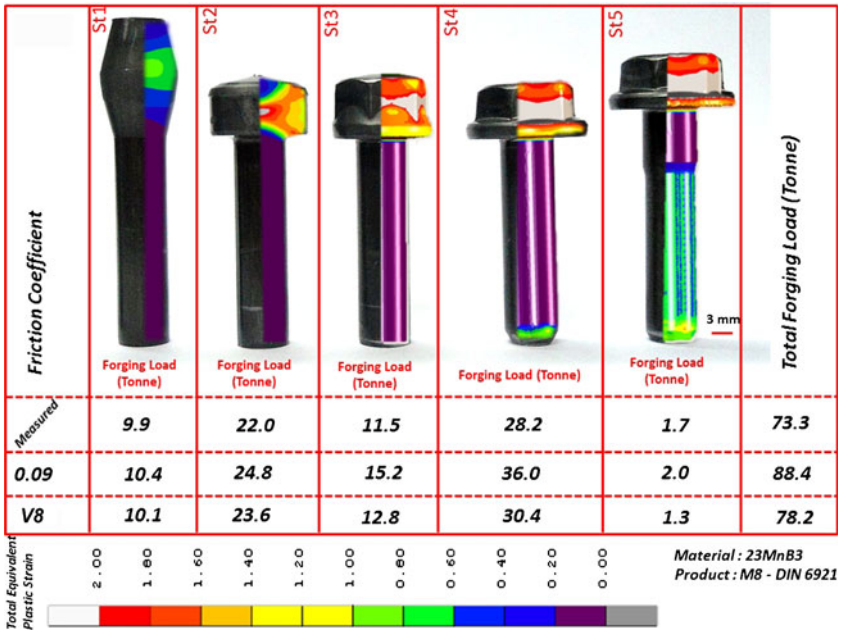

Fig. 18 The equivalent plastic strain distribution, forging loads, and total forging load of M8×30 DIN 6921 forging process

forging processes. The total forging loads with using temperature-dependent friction coefficients deviate from the measured total forging loads by 7, 16, 7, and 4 % for M8×28 plastic screw, M8×16 DIN 6921, M8×30 DIN 6921, and M8×65 bolt-forging processes, respectively. While, the deviations with the use of constant friction coefficients are sequentially 25, 38, 20, and 20 %. Except one forging process, the difference between simulation and measured total loads with the use of temperature-dependent friction coefficient is below 10 %. The results clearly dictate that the numerical forging loads predicted by the simulations using temperature-dependent friction coefficient approximate the measured loads closer than using constant friction coefficient. It is also noted in Fig. 20 that the differences between measured and numerically determined average forging loads increase with increasing forging loads. However, the differences are less pronounced with the use of temperature-dependent friction coefficient particularly at increasing forging loads as compared with the use of constant friction coefficient.

Figure 21 shows the variation of the friction coefficient with temperature. The determined set of friction coefficients noted in the same figure is relatively coarse between 200 and 300 and 300 and 400 °C and may require further numerical and experimental investigation of friction coefficients between these temperatures. In a previous study, the friction coefficient was reported to decrease with phosphate

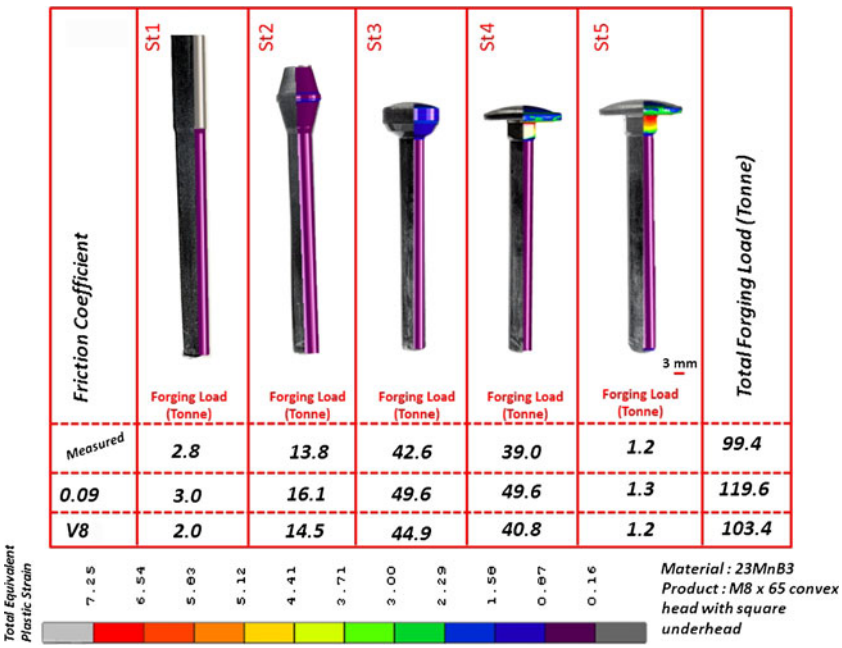

Fig. 19 The equivalent plastic strain distribution, forging loads, and total forging load of M8×65 convex head with square under head forging process

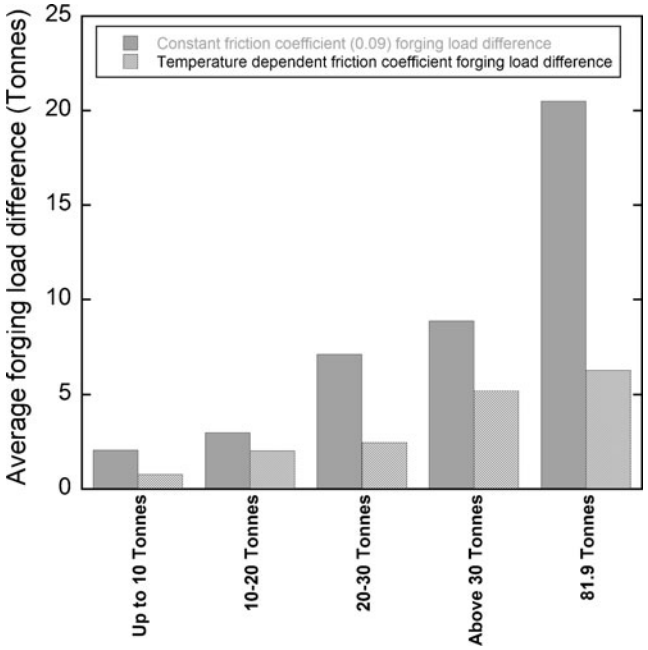

Fig. 20 Average differences between measured and numerically determined forging loads

coating with increasing temperature and attained a minimum value at 250–300 °C [12]. A friction coefficient of 0.04 at 150 °C was determined previously on a zinc phosphate/-soap-coated carbon steel [7], which agrees well with the determined friction coefficient at the same temperature. In another study, the friction coefficients on a zinc phosphate/-soap-coated steel at 150, 200, and 250 °C were reported to be 0.06, 0.05, and 0.04, respectively [13]. These friction coefficients also well agree with those of the present study; 0.04 and 0.035 between 100 and 200 °C. The increase of the friction coefficient after about 200–300 °C was further attributed to the decomposition or burning of the lubricant film [11, 12, 14].

The fidelity of the numerical results of the present study lies in partly the inclusion of the temperature-dependent

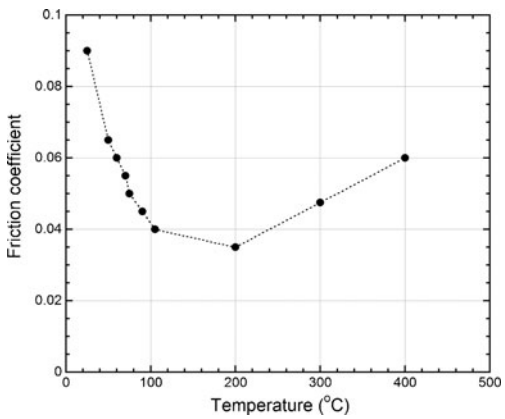

Fig. 21 The numerical variation of the friction coefficient with the forging temperature (V8 set)

friction coefficients and piece-wise temperature and strain rate-dependent flow stress material model into the fastener forging simulations and the use of a thermocoupling analysis based on the heat generation by plastic deformation and friction. However, the material thermal property variations with local temperature, pressure, and strain rate and the alterations in the heat conversion parameters with temperature and pressure may unavoidably affect the results. The used friction model further excludes the sticking of the lubricant between tool and workpiece which may eventually invalidates the dry slipping model used [15]. The heat generation factor was measured experimentally for several metals and found to range between 0.8 and 0.9, when the deformation was slip by the dislocation motion [16]. The factor decreased to a value of 0.6, when the twinning was the dominant deformation mechanism [17]. In most finite element programs, the factor is default and set to 0.9. Any local alterations in the deformation mechanism may naturally affect the numerical results.

The present experimental and numerical investigations showed that the use of temperature-dependent friction coefficients in thermo mechanical analysis decreases the load values in the order of 10 % as compared with constant friction coefficient and mechanical analysis. This may be advantage in deciding the load limits of the forging presses in the critical operations in which the total force is relatively high and in the level of the load capacity of the press.

5 Conclusions

A set of temperature-dependent friction coefficients was developed to increase the accuracy finite element simulations of cold bolt forging. The initially attained friction coefficients at different temperatures were calibrated with the iterations between the experimental and thermomechanical model extrusion test loads. The constant friction coefficient and the determined set of friction coefficients as function of temperature were then implemented to the simulations of the cold bolt-forging processes. Further calibrations and model validations were made based on the temperature measurements of the workpiece in the actual bolt forging of the M8×20 circular head and M10×20 Inbus DIN 912 bolt. To show the advantages of developed temperature-dependent friction coefficients, the loads of four different bolt-forging processes were compared with the thermomechanical model loads calculated using the constant friction and temperature-dependent friction coefficients. The results showed that variable friction coefficient thermomechanical analysis resulted in relatively lower total forging loads than the constant friction mechanical and thermomechanical analysis. Part of the decrease in total forging load resulted from the use of thermo mechanical

analysis as compared with mechanical analysis. The use of temperature-dependent friction coefficient in thermomechanical analysis decreased the load values in the order of 10 % as compared with constant friction coefficient and mechanical analysis.

Acknowledgments The authors would like to thank the Scientific and Technical Council of Turkey (TÜBITAK) for the grant # TEYDEB 3080689.

References

1. Hayhurst DR, Chan MW (2005) Determination of friction models for metallic die–workpiece interfaces. Int J Mech Sci 47(1):1–25
2. Behrens A, Schafstall H (1998) 2D and 3D simulation of complex multistage forging processes by use of adaptive friction coefficient. J Mater Process Technol 80–1:298–303
3. Cho HJ, Altan T (2005) Determination of flow stress and interface friction at elevated temperatures by inverse analysis technique. J Mater Process Technol 170(1–2):64–70. doi:10.1016/j.jmatprotec.2005.04.091
4. Wang JP, Lin FL, Huang BC, Yun CC (2008) A new experimental approach to evaluate friction in ring test. J Mater Process Technol 197(1–3):68–76. doi:10.1016/j.jmatprotec.2007.06.017
5. Cora ON, Akkok M, Darendeliler H (2008) Modelling of variable friction in cold forging. Proc Inst Mech Eng Part J-J Eng Tribol 222(J7):899–908. doi:10.1243/13506501jet419
6. Tan X, Bay N, Zhang W (2003) Friction measurement and modelling in forward rod extrusion tests. Proc Inst Mech Eng Part J-J Eng Tribol 217(J1):71–82
7. Dubois A, Lazzarotto L, Dubar L, Oudin J (2001) A multi-step lubricant evaluation strategy for wire drawing-extrusion-cold heading sequence. Wear 249(10–11):951–961
8. Saiki H, Ngaile G, Ruan LQ (1997) Influence of die geometry on the workability of conversion coatings combined with soap lubricant in cold forming of steels. J Mater Process Technol 63(1–3):238–243
9. Bay N (1994) The state of the art in cold forging lubrication. J Mater Process Technol 46(1–2):19–40. doi:10.1016/0924-0136(94)90100-7
10. Farias MCM, Santos CAL, Panossian Z, Sinatora A (2009) Friction behavior of lubricated zinc phosphate coatings. Wear 266(7–8):873–877. doi:10.1016/j.wear.2008.10.002
11. Weymueller R, Carl. (1962) Source book on cold forming; cold extrusion of steels: its promises and problems; American Society for Metals
12. Ruan LQ, Saiki H, Marumo Y, Imamura Y (2005) Evaluation of coating-based lubricants for cold forging using the localised rod-drawing test. Wear 259:1117–1122. doi:10.1016/j.wear.2005.02.103
13. Ngaile G, Saiki H, Ruan LQ, Marumo Y (2007) A tribo-testing method for high performance cold forging lubricants. Wear 262(5–6):684–692. doi:10.1016/j.wear.2006.08.009
14. Steenberg T, Olsen JS, Christensen E, Bjerrum NJ (1999) Estimation of temperature in the lubricant film during cold forging of stainless steel based on studies of phase transformations in the film. Wear 232(2):140–144. doi:10.1016/s0043-1648(99)00137-4
15. Tan X (2002) Comparisons of friction models in bulk metal forming. Tribol Int 35(6):385–393. doi:10.1016/S0301-679X(02)00020-8
16. Mason JJ, Rosakis AJ, Ravichandran G (1994) On the strain and strain rate dependence of the fraction of plastic work converted to heat: an experimental study using high speed infrared detectors and the Kolsky bar. Mech Mater 17(2–3):135–145
17. Meyers MA (1994) Dynamic behavior of materials. Wiley, New York